family formation predict that the memory of spin of the original unshattered parent body is lost[3], and existing models of spin angular momentum suggest that collisional evolution randomizes asteroid spin vectors regardless of their initial orientations[2], although the absolute timescale is uncertain. Here, I briefly identify two possible general explanations for future study.

One possibility is that randomly oriented gravitational aggregates from the initial collision have further fragmented, creating smaller objects that have the same spin obliquities as the remnants from which they were formed. Secondary fragmentation of the largest remnant of the initial break-up has previously been proposed to explain the existence of several objects of comparable size among the largest Koronis family members[16], but if the spin clusters were formed in this way then the absence of obvious corresponding associations in proper orbital elements also needs to be explained. To test this hypothesis, further work is needed to better understand the behaviour and evolution of gravitational aggregates.

A second possible explanation for spin clusters is that some dynamical process is aligning the obliquities and matching the rotation rates. Thermal effects can change obliquities and spin rates of small irregular asteroids, but calculations for Ida suggest that asteroids of comparable size are unlikely to have been substantially affected[17]. If a secular effect has clustered the spin vectors, then the present understanding of the timescale over which thermal processes have affected the spin cluster objects may be incomplete, or some nonthermal process may be at work. Finding similar clustering of spins for 20–40-km asteroids outside the Koronis family would support the hypothesis of a secular effect. □

Received 24 May; accepted 18 July 2002; doi:10.1038/nature00993.

1. Chapman, C. R., Paolicchi, P., Zappalà, V., Binzel, R. P. & Bell, J. F. in *Asteroids II* (eds Binzel, R. P., Gehrels, T. & Matthews, M. S.) 386–415 (Univ. Arizona Press, Tucson, 1989).
2. Binzel, R. P. Collisional evolution in the Eos and Koronis asteroid families: Observational and numerical results. *Icarus* **73,** 303–313 (1988).
3. Michel, P., Benz, W., Tanga, P. & Richardson, D. C. Collisions and gravitational reaccumulation: Forming asteroid families and satellites. *Science* **294,** 1696–1700 (2001).
4. Zappalà, V., Bendjoya, Ph., Cellino, A., Farinella, P. & Froeschle, C. Asteroid families: Search of a 12,487-asteroid sample using two different clustering techniques. *Icarus* **116,** 291–314 (1995).
5. Binzel, R. P. A photoelectric survey of 130 asteroids. *Icarus* **72,** 135–208 (1987).
6. Slivan, S. M. *Spin-Axis Alignment of Koronis Family Asteroids* PhD thesis, Massachusetts Institute of Technology (1995).
7. Slivan, S. M. & Binzel, R. P. Forty-eight new rotation lightcurves of 12 Koronis family asteroids. *Icarus* **124,** 452–470 (1996).
8. Slivan, S. M. *et al.* Spin vectors in the Koronis family: Comprehensive results from two independent analyses of 213 rotation lightcurves. *Icarus* (submitted).
9. Drummond, J. D., Weidenschilling, S. J., Chapman, C. R. & Davis, D. R. Photometric geodesy of main-belt asteroids. II. Analysis of lightcurves for poles, periods, and shapes. *Icarus* **76,** 19–77 (1988).
10. Kaasalainen, M. & Torppa, J. Optimization methods for asteroid lightcurve inversion. I. Shape determination. *Icarus* **153,** 24–36 (2001).
11. Kaasalainen, M., Torppa, J. & Muinonen, K. Optimization methods for asteroid lightcurve inversion. II. The complete inverse problem. *Icarus* **153,** 37–51 (2001).
12. Binzel, R. P. *et al.* Asteroid 243 Ida: Ground-based photometry and a pre-Galileo physical model. *Icarus* **105,** 310–325 (1993).
13. Davies, M. E. *et al.* The north pole direction and the control network of the asteroid 243 Ida. *Bull. Am. Astron. Soc.* **26,** 1154–1155 (1994).
14. Miller, I. & Freund, J. E. *Probability and Statistics for Engineers* (Prentice-Hall, Englewood Cliffs, New Jersey, 1977).
15. Belton, M. J. S. *et al.* First images of asteroid 243 Ida. *Science* **265,** 1543–1547 (1994).
16. Marzari, F., Davis, D. & Vanzani, V. Collisional evolution of asteroid families. *Icarus* **113,** 168–187 (1995).
17. Rubincam, D. P. Radiative spin-up and spin-down of small asteroids. *Icarus* **148,** 2–11 (2000).
18. Bowell, E., *et al.* in *Asteroids II* (eds Binzel, R. P., Gehrels, T. & Matthews, M. S.) 524–556 (Univ. Arizona Press, Tucson, 1989).
19. Landolt, A. U. *UVBRI* photometric standard stars around the celestial equator. *Astron. J.* **88,** 439–460 (1983).

Acknowledgements

I thank R. Binzel for advice and encouragement, and M. Kaasalainen, L. Crespo da Silva, M. Lyndaker and M. Krčo for contributions at various stages of this work.

Competing interests statement

The authors declare that they have no competing financial interests.

Correspondence and requests for materials should be addressed to the author (e-mail: slivan@mit.edu).

Collapse and revival of the matter wave field of a Bose–Einstein condensate

Markus Greiner, Olaf Mandel, Theodor W. Hänsch & Immanuel Bloch

Sektion Physik, Ludwig-Maximilians-Universität, Schellingstrasse 4/III, D-80799 Munich, Germany, and Max-Planck-Institut für Quantenoptik, D-85748 Garching, Germany

A Bose–Einstein condensate represents the most 'classical' form of a matter wave, just as an optical laser emits the most classical form of an electromagnetic wave. Nevertheless, the matter wave field has a quantized structure owing to the granularity of the discrete underlying atoms. Although such a field is usually assumed to be intrinsically stable (apart from incoherent loss processes), this is no longer true when the condensate is in a coherent superposition of different atom number states[1–6]. For example, in a Bose–Einstein condensate confined by a three-dimensional optical lattice, each potential well can be prepared in a coherent superposition of different atom number states, with constant relative phases between neighbouring lattice sites. It is then natural to ask how the individual matter wave fields and their relative phases evolve. Here we use such a set-up to investigate these questions experimentally, observing that the matter wave field of the Bose–Einstein condensate undergoes a periodic series of collapses and revivals; this behaviour is directly demonstrated in the dynamical evolution of the multiple matter wave interference pattern. We attribute the oscillations to the quantized structure of the matter wave field and the collisions between individual atoms.

In order to determine the evolution with time of a many-atom state with repulsive interactions in a confining potential, we first assume that all atoms occupy only the ground state of the external potential. The hamiltonian governing the system after subtracting the ground-state energy of the external potential is then solely determined by the interaction energy between the atoms:

$$\hat{H} = \frac{1}{2}U\hat{n}(\hat{n}-1) \qquad (1)$$

Here $\hat{n}$ counts the number of atoms in the confining potential, and U is the on-site interaction matrix element that characterizes the energy cost due to the repulsive interactions when a second atom is added to the potential well. It can be related to the s-wave scattering length a and the ground-state wavefunction $w(\mathbf{x})$ through $U = 4\pi\hbar^2 a/m \int |w(\mathbf{x})|^4 \, \mathrm{d}^3x$, as long as the vibrational level spacing of the external potential is large compared with the interaction energy. The eigenstates of the above hamiltonian are Fock states $|n\rangle$ in the atom number, with eigenenergies $E_n = Un(n-1)/2$. The evolution with time (t) of such an n-particle state is then simply given by $|n\rangle(t) = |n\rangle(0) \times \exp(-iE_n t/\hbar)$, where $\hbar$ is Planck's constant (h) divided by 2π.

We now consider a coherent state $|\alpha\rangle$ (see, for example, ref. 7) of the atomic matter field in a potential well. Such a coherent state with a complex amplitude α and an average number of atoms $\bar{n} = |\alpha|^2$ can be expressed as a superposition of different number states $|n\rangle$ such that $|\alpha\rangle = \exp(-|\alpha|^2/2)\sum_n \frac{\alpha^n}{\sqrt{n!}}|n\rangle$. Now the system is in a superposition of different eigenstates, which evolve in time according to their eigenenergies E_n. This allows us to calculate the evolution with time of an initially coherent state:

$$|\alpha\rangle(t) = \mathrm{e}^{-|\alpha|^2/2}\sum_n \frac{\alpha^n}{\sqrt{n!}}\mathrm{e}^{-i\frac{1}{2}Un(n-1)t/\hbar}|n\rangle \qquad (2)$$

Evaluating the atomic field operator $\hat{a}$ for such a state then yields the

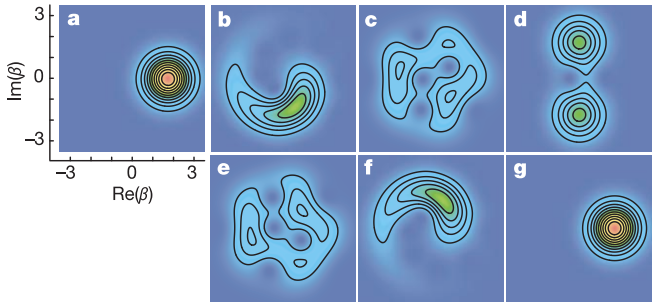

Figure 1 Quantum dynamics of a coherent state owing to cold collisions. The images **a**–**g** show the overlap $|\langle\beta|\alpha(t)\rangle|^2$ of an arbitrary coherent state $|\beta\rangle$ with complex amplitude β with the dynamically evolved quantum state $|\alpha\rangle(t)$ (see equation (2)) for an average number of $|\alpha|^2 = 3$ atoms at different times t. **a**, $t = 0\,h/U$; **b**, 0.1 h/U; **c**, 0.4 h/U; **d**, 0.5 h/U; **e**, 0.6 h/U; **f**, 0.9 h/U; and **g**, h/U. Initially, the phase of the macroscopic matter wave field becomes more and more uncertain as time evolves (**b**), but remarkably at $t_{rev}/2$ (**d**), when the macroscopic field has collapsed such that $\psi \approx 0$, the system has evolved into an exact 'Schrödinger cat' state of two coherent states. These two states are 180° out of phase, and therefore lead to a vanishing macroscopic field ψ at these times. More generally, we can show that at certain rational fractions of the revival time t_{rev}, the system evolves into other exact superpositions of coherent states—for example, at $t_{rev}/4$, four coherent states, or at $t_{rev}/3$, three coherent states[2,4]. A full revival of the initial coherent state is then reached at $t = h/U$. In the graph, red denotes maximum overlap and blue vanishing overlap with 10 contour lines in between.

macroscopic matter wave field $\psi = \langle\alpha(t)|\hat{a}|\alpha(t)\rangle$, which has an intriguing dynamical evolution. At first, the different phase evolutions of the atom number states lead to a collapse of ψ. However, at integer multiples of the revival time $t_{rev} = h/U$ all phase factors in the sum of equation (2) re-phase modulo 2π, leading to a perfect revival of the initial coherent state. The collapse time t_c depends on the variance σ_n^2 of the atom number distribution, such that $t_c \approx t_{rev}/\sigma_n$ (see refs 1–5). A more detailed picture of the dynamical evolution of ψ can be seen in Fig. 1, where the overlap of an arbitrary coherent state $|\beta\rangle$ with the state $|\alpha\rangle$ (t) is shown for different evolution times up to the first revival time of the many-body state[8,9].

In our experiment, we create coherent states of the matter wave field in a potential well, by loading a magnetically trapped Bose–Einstein condensate into a three-dimensional optical lattice potential. For low potential depths, where the tunnelling energy J is much larger than the on-site repulsive interaction energy U in a single well, each atom is spread out over all lattice sites. For the case of a homogeneous system with N atoms and M lattice sites, the many-body state can then be written in second quantization as a product of identical single-particle Bloch waves with zero quasi-momentum $|\Psi\rangle_{U/J=0} \propto \left(\sum_{i=1}^{M} \hat{a}_i^\dagger\right)^N |0\rangle$. It can be approximated by a product over single-site many-body states $|\phi_i\rangle$, such that $|\Psi\rangle_{U/J=0} \approx \prod_{i=1}^{M} |\phi_i\rangle$. In the limit of large N and M, the atom number distribution of $|\phi_i\rangle$ in each potential well is poissonian and almost identical to that of a coherent state. Furthermore, all the matter waves in different potential wells are phase coherent, with constant relative phases between lattice sites. As the lattice potential depth V_A is increased and J decreases, the atom number distribution in each potential well becomes markedly subpoissonian[10] owing to the repulsive interactions between the atoms, even before entering the Mott insulating state[11–13]. After preparing superposition states $|\phi_i\rangle$ in each potential well, we increase the lattice potential depth rapidly in order to create isolated potential wells. The hamiltonian of equation (1) then determines the dynamical evolution of each of these potential wells.

The experimental set-up used here to create Bose–Einstein condensates in the three-dimensional lattice potential (see Methods) is similar to that used in our previous work[11,14,15]. Briefly, we start with a quasi-pure Bose–Einstein condensate of up to 2×10^5 ^{87}Rb atoms in the $|F = 2, m_F = 2\rangle$ state in a harmonic magnetic trapping potential with isotropic trapping frequencies of $\omega = 2\pi \times 24$ Hz. Here F and m_F denote the total angular momentum

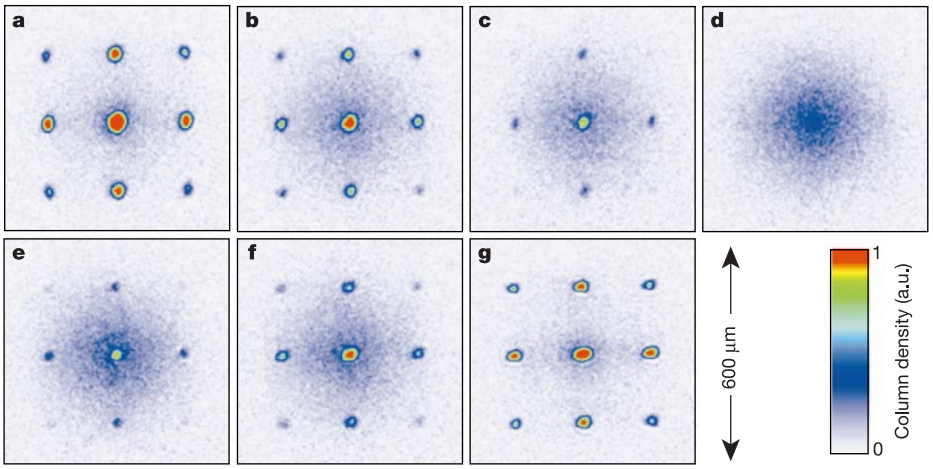

Figure 2 Dynamical evolution of the multiple matter wave interference pattern observed after jumping from a potential depth $V_A = 8\ E_r$ to a potential depth $V_B = 22\ E_r$ and a subsequent variable hold time t. After this hold time, all trapping potentials were shut off and absorption images were taken after a time-of-flight period of 16 ms. The hold times t were **a**, 0 μs; **b**, 100 μs; **c**, 150 μs; **d**, 250 μs; **e**, 350 μs; **f**, 400 μs; and **g**, 550 μs. At first, a distinct interference pattern is visible, showing that initially the system can be described by a macroscopic matter wave with phase coherence between individual potential wells. Then after a time of ~250 μs the interference pattern is completely lost. The vanishing of the interference pattern is caused by a collapse of the macroscopic matter wave field in each lattice potential well. But after a total hold time of 550 μs (**g**) the interference pattern is almost perfectly restored, showing that the macroscopic matter wave field has revived. The atom number statistics in each well, however, remains constant throughout the dynamical evolution time. This is fundamentally different from the vanishing of the interference pattern with no further dynamical evolution, which is observed in the quantum phase transition to a Mott insulator, where Fock states are formed in each potential well. From the above images the number of coherent atoms N_{coh} is determined by first fitting a broad two-dimensional gaussian function to the incoherent background of atoms. The fitting region for the incoherent atoms excludes 130 μm × 130 μm squares around the interference peaks. Then the number of atoms in these squares is counted by a pixel-sum, from which the number of atoms in the incoherent gaussian background in these fields is subtracted to yield N_{coh}. a.u., arbitrary units.

and the magnetic quantum number of the atom's hyperfine state. In order to transfer the magnetically trapped atoms into the optical lattice potential, we slowly increase the intensity of the lattice laser beams over a time of 80 ms so that a lattice potential depth V_A of up to 11 recoil energies E_r (see Methods) is reached[11]. This value of V_A is chosen so that the system is still completely in the superfluid regime[16]. We then rapidly increase the lattice potential depth to a value V_B of up to 35 E_r within a time of 50 μs so that the tunnel coupling between neighbouring potential wells becomes negligible. The timescale for the jump in the potential depth is chosen such that it is fast compared with the tunnelling time between neighbouring potential wells, but sufficiently slow to ensure that all atoms remain in the vibrational ground state of each well. In this way, we preserve the atom number distribution of the potential depth V_A at the potential depth V_B.

We follow the dynamical evolution of the matter wave field after jumping to the potential depth V_B by holding the atoms in the optical lattice for different times t. After these hold times, we suddenly turn off the confining optical and magnetic trapping potentials and observe the resulting multiple matter wave interference pattern after a time-of-flight period of 16 ms. An example of such an evolution can be seen in Fig. 2, which shows the collapse and revival of the interference pattern over a time of 550 μs. This collapse and revival of the interference pattern is directly related to the collapses and revivals of the individual coherent matter wave fields in each potential well. It is important to note a crucial difference between the outcome of a collapse and revival experiment in a double-well system and our multiple-well system. In a double-well system, a perfect interference pattern would be observed in each single realization of the experiment for all times. However, when the matter wave fields have collapsed in both wells, this interference pattern would alternate randomly for each realization. Averaging over several single realizations would then yield the ensemble average value $\psi = 0$ that indicates the randomness of the interference pattern associated with the collapse of the matter wave fields. For the multiple-well set-up used here, however, the interference pattern in a single realization of the experiment can only be observed if the matter wave fields in each potential well have constant relative phase to each other, which requires that $\psi \neq 0$. The matter wave field ψ is therefore directly connected to the visibility of the multiple matter wave interference pattern in a single realization of the experiment.

In order to analyse quantitatively the temporal evolution of the interference pattern, we evaluate the number of atoms in the first and central order interference peaks N_{coh} versus the total number of atoms N_{tot} in the time-of-flight images. In the optical lattice, the matter wave field in each potential well $\psi_i(t) = \langle\phi_i(t)|\hat{a}_i|\phi_i(t)\rangle$ collapses and revives owing to the nonlinear dynamics discussed above. In order to relate the time evolution of the global fraction of coherent atoms N_{coh}/N_{tot} to such a single-site time evolution $\psi_i(t)$ with $\bar{n}_i$ atoms on average on this lattice site, we sum the coherent fraction in each well over all M lattice sites: $N_{coh}/N_{tot} = 1/N_{tot}\sum_{i=1}^{M}|\psi_i(t)|^2$. This sum can be converted into an integral using the classical probability distribution $W(\bar{n})$ which describes the probability of finding a lattice site with an average number of $\bar{n}$ atoms. If the single-site dynamics is given by $\psi(t,\bar{n},(U/J)_A,U_B)$, then the total number of coherent atoms can be determined by $N_{coh} = \int W(\bar{n})|\psi(t,\bar{n},(U/J)_A,U_B)|^2\,d\bar{n}$. Using the Bose–Hubbard model and assuming a homogenous system, we are able to numerically calculate the initial atom number statistics on a single lattice site for finite U/J up to $U/J \approx 20$ and small $\bar{n}$ using a Gutzwiller ansatz[13,17]. This allows us to predict the dynamical evolution of the matter wave field on a single lattice site $\psi(t,\bar{n},(U/J)_A,U_B)$. Figure 3 shows the experimentally determined evolution of N_{coh}/N_{tot} over time after jumping to the potential depth V_B. Up to five revivals are visible, after which a damping of the signal prevents further detection of revivals.

The revival of the matter wave field in each potential well is expected to occur at times that are multiples of h/U, independent of the atom number statistics in each well. Therefore, in our inhomogeneous system, the macroscopic interference pattern should revive at the same times on all sites. As the on-site matrix element U increases for greater potential depths, we expect the revival time to decrease as V_B increases. This is shown in Fig. 4, where we have measured the revival period for different final potential depths V_B. We find excellent agreement between an *ab initio* calculation of h/U

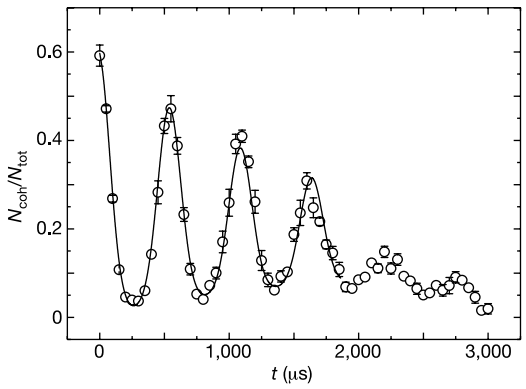

Figure 3 Number of coherent atoms relative to the total number of atoms monitored over time for the same experimental sequence as in Fig. 2. The solid line is a fit to the data assuming a sum of gaussians with constant widths and constant time separations, including an exponential damping and a linear background. The damping is mainly due to the following process: after jumping to a potential depth V_B and thereby abruptly changing the external confinement and the on-site matrix element U, we obtain a parabolic profile of the chemical potential over the cloud of atoms in the optical lattice, which leads to a broadening of the interference peaks over time. When the interference peaks become broader than the rectangular area in which they are counted, we cannot determine N_{coh} correctly any more, which explains the rather abrupt damping that can be seen—for example, between the third and fourth revival in the above figure. Furthermore, the difference in U of ~3% over the cloud of atoms contributes to the damping of N_{coh}/N_{tot} over time. The finite contrast in N_{coh}/N_{tot} of initially 60% can be attributed to atoms in higher-order momentum peaks (~10% of the total atom number), *s*-wave scattering spheres created during the expansion[14], a quantum depletion of the condensate for the initial potential depth of $V_A = 8\ E_r$, and a finite condensate fraction due to the finite temperature of the system.

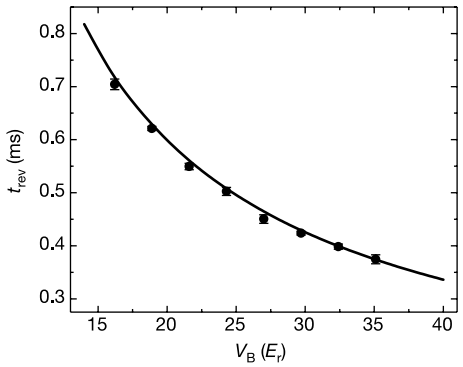

Figure 4 Revival period in the dynamical evolution of the interference pattern after jumping to different potential depths V_B from a potential depth of $V_A = 5.5\ E_r$. The solid line is an *ab initio* calculation of h/U with no adjustable parameters based on a band structure calculation. In addition to the statistical uncertainties shown in the revival times, the experimental data points have a systematic uncertainty of 15% in the values for the potential depth.

from a band structure calculation and our data points. The revivals also directly prove the quantization of the underlying Bose field, and provide experimental proof that collisions between atoms lead to a fully coherent collisional phase $Un(n-1)t/2\hbar$ of the $|n\rangle$-particle state over time, even on the level of individual pairs of atoms.

As we increase our initial lattice potential depth V_A, we expect the atom number distribution in each well to become markedly sub-poissonian owing to the increasing importance of the interactions as U/J increases. This in turn should lead to an increase of the collapse time, which depends on the variance of the superimposed number states. We have verified this by measuring the collapse time for different values of V_A (Fig. 5a). We can clearly observe a significant increase in the collapse time, when jumping from greater potential depths. For example, when jumping from $V_A = 11\ E_r$, t_c/t_{rev} is more than 50% larger than when jumping from $V_A = 4\ E_r$. This indicates that the atom number distribution in each potential well has indeed become subpoissonian, because for our experimental parameters the average atom number per lattice site, $\bar{n}_i$ remains almost constant when V_A is increased. A comparison of the collapse time for different initial potential depths V_A to a theoretical prediction is shown in Fig. 5b.

The observed collapse and revival of the macroscopic matter wave field of a Bose–Einstein condensate directly demonstrate behaviour of ultracold matter beyond mean-field theories. Furthermore, the collapse times can serve as an independent, efficient probe of the atom number statistics in each potential well. It would be interesting to start from a Mott insulating state and use the coherent collisions between single atoms, which have been demonstrated here, to create a many-atom entangled state[18–20]. This highly entangled state could then serve as a promising starting point for quantum computing with neutral atoms[19,21]. □

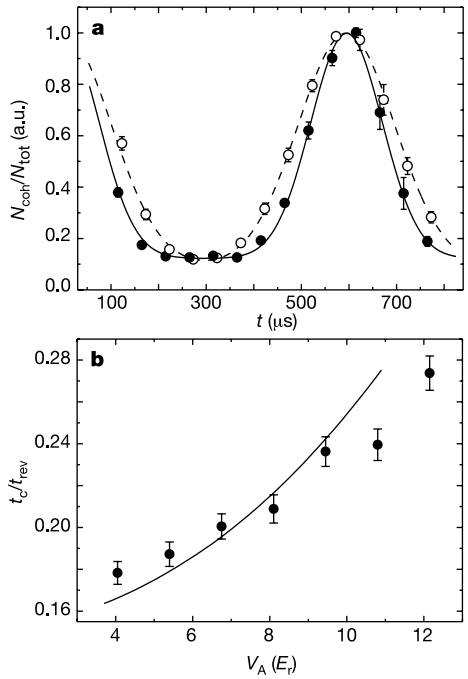

Figure 5 Influence of the atom number statistics on the collapse time. **a**, First revival observed in the ratio N_{coh}/N_{tot} after jumping from different initial potential depths $V_A = 4\ E_r$ (filled circles) and $V_A = 11\ E_r$ (open circles) to a potential depth of $V_B = 20\ E_r$. The data have been scaled to the same height in order to compare the widths of the collapse times, where the contrast of the curve at $V_A = 11\ E_r$ was 20% smaller than that for $V_A = 4\ E_r$. The solid and dashed line are fits to the data assuming a sum of two gaussians with constant widths t_c (measured as the 1/e half width of the gaussian), spaced by the corresponding revival time t_{rev} for the potential depth $V_B = 20\ E_r$. **b**, Collapse time t_c relative to the revival time t_{rev} after jumping from different potential depths V_A to a potential depth $V_B = 20\ E_r$. The solid line is an *ab initio* theoretical prediction based on the averaged time-evolution of the matter wave fields in each lattice potential well described in the text. Considering the systematic experimental uncertainties in the determination of the potential depths V_A of ~15% and an uncertainty in the total atom number of ~20%, we find a reasonable agreement between both the experimental data and the theoretical prediction. a.u., arbitrary units.

Methods

Optical lattices

A three-dimensional array of microscopic potential wells is created by overlapping three orthogonal optical standing waves at the position of the Bose–Einstein condensate. The atoms are then trapped in the intensity maxima of the standing-wave light field owing to the resulting dipole force. The laser beams for the periodic potential are operated at a wavelength of $\lambda = 838$ nm with beam waists of ~125 μm at the position of the Bose–Einstein condensate. This gaussian laser beam profile leads to an additional isotropic harmonic confinement of the atoms with trapping frequencies of 60 Hz for lattice potential depths of 20 E_r. Here E_r denotes the recoil energy $E_r = \hbar^2k^2/2m$, with $k = 2\pi/\lambda$ being the wavevector of the laser light and m the mass of a single atom. In this configuration, we populate almost 150,000 lattice sites with an average atom number per lattice site of up to 2.5 in the centre of the lattice. The lattice structure is of simple cubic type, with a lattice spacing of $\lambda/2$ and oscillation frequencies in each lattice potential well of ~30 kHz for a potential depth of 20 E_r.

Received 9 April; accepted 4 July 2002; doi:10.1038/nature00968.

1. Wright, E. M., Walls, D. F. & Garrison, J. C. Collapses and revivals of Bose-Einstein condensates formed in small atomic samples. *Phys. Rev. Lett.* **77,** 2158–2161 (1996).
2. Wright, E. M., Wong, T., Collett, M. J., Tan, S. M. & Walls, D. F. Collapses and revivals in the interference between two Bose-Einstein condensates formed in small atomic samples. *Phys. Rev. A* **56,** 591–602 (1997).
3. Imamoglu, A., Lewenstein, M. & You, L. Inhibition of coherence in trapped Bose-Einstein condensates. *Phys. Rev. Lett.* **78,** 2511–2514 (1997).
4. Castin, Y. & Dalibard, J. Relative phase of two Bose-Einstein condensates. *Phys. Rev. A* **55,** 4330–4337 (1997).
5. Dunningham, J. A., Collett, M. J. & Walls, D. F. Quantum state of a trapped Bose-Einstein condensate. *Phys. Lett. A* **245,** 49–54 (1998).
6. Zhang, W. & Walls, D. F. Bosonic-degeneracy-induced quantum correlation in a nonlinear atomic beam splitter. *Phys. Rev. A* **52,** 4696–4703 (1995).
7. Walls, D. F. & Milburn, G. J. *Quantum Optics* (Springer, Berlin, 1994).
8. Milburn, G. J. & Holmes, C. A. Dissipative quantum and classical Liouville mechanics of the anharmonic oscillator. *Phys. Rev. Lett.* **56,** 2237–2240 (1986).
9. Daniel, D. J. & Milburn, G. J. Destruction of quantum coherence in a nonlinear oscillator via attenuation and amplification. *Phys. Rev. A* **39,** 4628–4640 (1989).
10. Orzel, C., Tuchman, A. K., Fenselau, M. L., Yasuda, M. & Kasevich, M. A. Squeezed states in a Bose-Einstein condensate. *Science* **291,** 2386–2389 (2001).
11. Greiner, M., Mandel, O., Esslinger, T., Hänsch, T. W. & Bloch, I. Quantum phase transition from a superfluid to a Mott insulator in a gas of ultracold atoms. *Nature* **415,** 39–44 (2002).
12. Fisher, M. P. A., Weichman, P. B., Grinstein, G. & Fisher, D. S. Boson localization and the superfluid-insulator transition. *Phys. Rev. B* **40,** 546–570 (1989).
13. Jaksch, D., Bruder, C., Cirac, J. I., Gardiner, C. W. & Zoller, P. Cold bosonic atoms in optical lattices. *Phys. Rev. Lett.* **81,** 3108–3111 (1998).
14. Greiner, M., Bloch, I., Mandel, O., Hänsch, T. W. & Esslinger, T. Exploring phase coherence in a 2D lattice of Bose-Einstein condensates. *Phys. Rev. Lett.* **87,** 160405-1–160405-4 (2001).
15. Greiner, M., Bloch, I., Hänsch, T. W. & Esslinger, T. Magnetic transport of trapped cold atoms over a large distance. *Phys. Rev. A* **63,** 031401-1–031401-4 (2001).
16. Cataliotti, F. S. *et al.* Josephson junction arrays with Bose-Einstein condensates. *Science* **293,** 843–846 (2001).
17. Rokhsar, D. S. & Kotliar, B. G. Gutzwiller projection for bosons. *Phys. Rev. B* **44,** 10328–10332 (1991).
18. Jaksch, D., Briegel, H. J., Cirac, J. I., Gardiner, C. W. & Zoller, P. Entanglement of atoms via cold controlled collisions. *Phys. Rev. Lett.* **82,** 1975–1978 (1999).
19. Briegel, H. J., Calarco, T., Jaksch, D., Cirac, J. I. & Zoller, P. Quantum computing with neutral atoms. *J. Mod. Opt.* **47,** 415–451 (2000).
20. Briegel, H. J. & Raussendorf, R. Persistent entanglement in arrays of interacting particles. *Phys. Rev. Lett.* **86,** 910–913 (2001).
21. Raussendorf, R. & Briegel, H. J. A one-way quantum computer. *Phys. Rev. Lett.* **86,** 5188–5191 (2001).

Acknowledgements

We thank W. Zwerger, T. Esslinger, A. Görlitz, H. Briegel, E. Wright and I. Cirac for discussions, and A. Altmeyer for help in the final stages of the experiment. This work was supported by the DFG.

Competing interests statement

The authors declare that they have no competing financial interests.

Correspondence and requests for materials should be addressed to I.B. (e-mail: imb@mpq.mpg.de).

